Large Tunneling Magnetoresistance in non-volatile 2D Hybrid Spin Filters

Xiaoyu Wang,[1,*] Lihao Zhang,[1,*] Miao He,[2,3] Qi Li,[4] Wenqin Song,[5] Kunlin Yang,[5] Shuxi Wang,[1] Takashi Taniguchi,[6] Kenji Watanabe,[7] Lei Zhang,[1] Wu Shi,[5,8,†] Yingchun Cheng,[9] Zhe Qu,[2,3] Jie Pan,[1,‡] and Zhe Wang[1,§]

[1] *MOE Key Laboratory for Nonequilibrium Synthesis and Modulation of Condensed Matter, Shaanxi Province Key Laboratory of Advanced Materials and Mesoscopic Physics, School of Physics, Xi'an Jiaotong University, Xi'an,710049, China*

[2] *Anhui Key Laboratory of Low-Energy Quantum Materials and Devices, High Magnetic Field Laboratory, Hefei Institutes of Physical Science,Chinese Academy of Sciences, Hefei 230031, China*

[3] *Science Island Branch of Graduate School, University of Science and Technology of China, Hefei 230026, China*

[4] *Key Laboratory of Flexible Electronics and Institute of Advanced Materials, Nanjing Tech University, Nanjing 211816, China*

[5] *State Key Laboratory of Surface Physics and Institute for Nanoelectronic Devices and Quantum Computing, Fudan University, Shanghai 200433, China*

[6] *Research Center for Materials Nanoarchitectonics, National Institute for Materials Science, Tsukuba 305-0044, Japan*

[7] *Research Center for Electronic and Optical Materials, National Institute for Materials Science, Tsukuba 305-0044, Japan*

[8] *Zhangjiang Fudan International Innovation Center, Fudan University, Shanghai 201210, China*

[9] *State Key Lab of Metastable Materials Science and Technology, Yanshan University, Qinhuangdao 066004, China*

Ferromagnetic semiconductors offer an efficient way to achieve high spin polarization via spin filtering effect. Large tunneling magnetoresistance (TMR) can then be realized when multiple spin filters are put in series, as recently demonstrated in van der Waals 2D A-type antiferromagnets such as CrI_3 and CrSBr. However, the interlayer antiferromagnetic ground state of these magnets inherently results in a high resistance state at zero field, this volatile behavior limits potential applications. Here we fabricate hybrid spin filters using 2D ferromagnetic metal Fe_3GeTe_2 and semiconductor $CrBr_3$, which are non-volatile as two magnets are magnetically decoupled. We achieve large TMR of around 100%, with its temperature dependence well fitted by the extended Jullière model. Additionally, the devices allow spin injection tuned through bias voltage and TMR polarity reversals are observed. Our work opens a new route to develop 2D magnetic semiconductor based spintronics.

Spintronic devices are increasingly pivotal in modern information technologies due to their non-volatile nature and low power consumption. The tunneling magnetoresistance (TMR) effect, which produces distinct resistance states representing 0 and 1 in digital world, is the basis for the operation of spintronic devices [1–3]. Highly spin-polarized current is paramount to achieve substantial TMR, which is conventionally generated from ferromagnetic metals with spin-polarized density of states (DOS) as in magnetic tunnel junctions [1, 3, 4]. It can also be achieved through spin filters composed of ferromagnetic semiconductors [5], whose spin-split bands result in different tunneling barrier heights for spin-up and spin-down electrons. Although pioneering studies have explored spin filters in systems like europium chalcogenides [6, 7], manganites [8–10], ferrites [11–13], the TMR data quality has not matched that of conventional magnetic tunnel junctions, mainly due to the lack of high quality magnetic semiconductors and heterostructure interfaces in ultra-thin devices.

The emergence of van der Waals (vdW) 2D magnets [14, 15] offers an exciting platform for utilizing spin filtering effects, as these 2D materials maintain high quality even in monolayer form and easily form heterostructures with atomically sharp interfaces. Previous investigations of vdW 2D A-type antiferromagnetic semiconductors such as CrI_3 [16–19], $CrCl_3$ [20–22], $CrPS_4$ [23] and CrSBr [24] have demonstrated very large TMR through spin filtering effects. These 2D antiferromagnets serve as multiple spin filters that are naturally in series and large TMR is produced when interlayer magnetic coupling is modified by the magnetic field. However, the antiferromagnetic ground state inherently results in a high resistance state at zero field, that is, a volatile behavior.

We propose a solution to this challenge by realizing 2D hybrid spin filters with one vdW ferromagnetic semiconductor as tunneling barrier, one vdW ferromagnetic metal and one normal metal as electrodes. It utilizes both the spin filtering effect of the ferromagnetic semiconductor and the spin-polarized DOS of the ferromagnetic metal to achieve large TMR. We consider the spin polarization of ferromagnetic metal to be positive, as shown in Fig. 1(a). When magnetizations of the ferromagnetic metal and semiconductor are in the parallel configuration, the majority-spin electrons of the ferromagnetic metal can tunnel through the lower barrier formed by the majority-spin electrons of ferromagnetic semiconductor, leading to a low resistance. Conversely, in the antiparallel configuration, a higher tunneling barrier for the majority-spin electrons of the ferromagnetic metal leads to a high resistance. Most importantly, the device operates in a non-volatile manner as the ferromagnetic metal and ferromagnetic semiconductor are magnetically decoupled,

* These authors contribute equally to this work.
† shiwu@fudan.edu.cn
‡ jiepan@xjtu.edu.cn
§ zhe.wang@xjtu.edu.cn

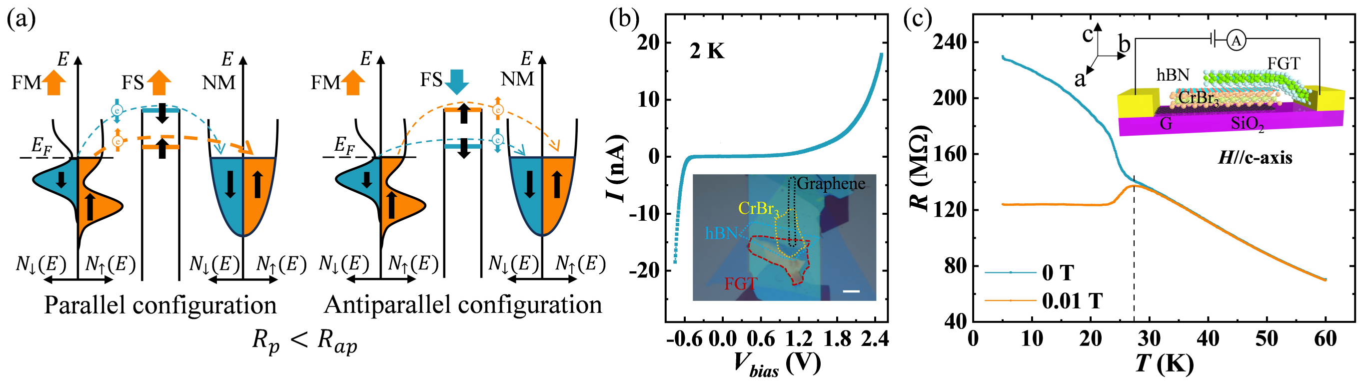

FIG. 1. **Basic characteristics of 2D Hybrid Spin Filter of Fe_3GeTe_2/hBN/$CrBr_3$/graphene.** **(a)** Spin dependent tunneling in hybrid spin filter, composed of ferromagnetic metal (FM), ferromagnetic semiconductor (FS) and normal metal (NM). When the magnetizations of FM and FS are in the parallel configuration (the left image), the device is in the low resistance state as the majority-spin electrons of FM tunnel through the lower barrier of FS. The device will be moved into the high resistance state when the magnetizations of two magnets are in the antiparallel configuration. **(b)** *IV* curve of Fe_3GeTe_2/hBN/$CrBr_3$/Graphene, whose optical image is shown in the inset with white scale bar of 5 µm. From optical contrast, $CrBr_3$ is around 3-layer , FGT is around 15-layer in thickness and the isolating hBN between them is around 4-layer. The measurement is done at 2 K and the graphene electrode is grounded. **(c)** Temperature dependence of tunneling resistance with zero field and 0.01 T field cooling process, measured with bias voltage of -0.66 V. Field of 0.01 T is used to ensure the device is in the parallel configuration, the dashed line of 27 K indicates the critical temperature of $CrBr_3$ flake. The inset shows the schematic image of the device.

which can be further ensured by inserting a thin insulator between two magnets. The functionality of the hybrid spin filter can be further enriched by employing an A-type antiferromagnetic semiconductor as a tunneling barrier, as more than two resistance states can be obtained. In this work, we report the realization of a 2D hybrid spin filter comprising Fe_3GeTe_2/hBN/$CrBr_3$/Graphene heterostructures. We achieve large TMR in this non-volatile device, then demonstrated the ability to tune TMR and even reverse its polarity via bias voltage.

Here we use Fe_3GeTe_2 (FGT) as the vdW 2D ferromagnetic metal electrode, whose Curie temperature is around 220 K in bulk and lower in atomically thin layers [25, 26]. It has been used to realize high-quality 2D magnetic tunnel junctions and demonstrate large spin polarization [27–30]. We use vdW ferromagnetic semiconductor $CrBr_3$ as the tunneling barrier. The Curie temperature of bulk $CrBr_3$ is around 32 K and decreases as the thickness decreases [31–33]. The spin-split band of $CrBr_3$ is theoretically expected [34, 35] and has been verified in recent electronic transport measurements [33, 36]. Its spin splitting energy is found to be proportional to its magnetization [36]. Stacking faults in $CrBr_3$ flakes will result in local interlayer coupling to be antiferromagnetic in that part [37–39]. We use multilayer graphene as the normal metal electrode in 2D hybrid spin filters, and insert atomically thin hBN between FGT and $CrBr_3$ to ensure that they are magnetically decoupled. Thus, the entire device is assembled with purely vdW 2D materials, securing high-quality interfaces which are crucial for achieving large TMR. As FGT and $CrBr_3$ are sensitive to air, the flake exfoliations and vdW heterostructure assembly were carried out in a nitrogen-filled glove box. The insets of Fig. 1(b) and Fig. 1(c) show the optical and schematic images of the hybrid spin filter, respectively. In the following, we present data from a representative device, with similar data from another device included in Supplementary Material [40].

Fig. 1(b) shows the current versus voltage (*IV*) of FGT/hBN/$CrBr_3$/Graphene measured at 2 K, with the graphene electrode grounded. The *IV* is non-linear and non-symmetric with respect to zero voltage, as expected for an asymmetric tunnel junction. Fig. 1(c) shows the temperature dependence of the tunneling resistance (*RT* curve) measured with -0.66 V. The blue line represents the measurement with zero field cooling, with a clear feature observed at around 27 K, indicating the critical temperature of our $CrBr_3$ flake (around 3-layer). The orange line represents the measurement with a 0.01 T field cooling, setting the preferred magnetization direction of FGT and $CrBr_3$ so that the device can be in parallel configuration. Two *RT* curves merge with each other above the critical temperature of 27 K and diverge below that temperature. These indicate that the spin configuration impacts the resistance of the whole device.

We measured the tunneling resistance with magnetic field applied along the easy axis (c-axis) of FGT and $CrBr_3$ at 2 K, and spin-valve-like TMR behavior is clearly observed. As shown in Fig. 2(a), when the magnetic field is swept from a large positive value to a negative value (indicated as the blue line), the tunneling resistance slightly changes from 2 T to zero field, but suddenly reaches a high resistance value at around -0.02 T. The high resistance state continues until the magnetic field reaches -0.5 T, where the resistance of the junction suddenly drops to its low resistance state. The TMR

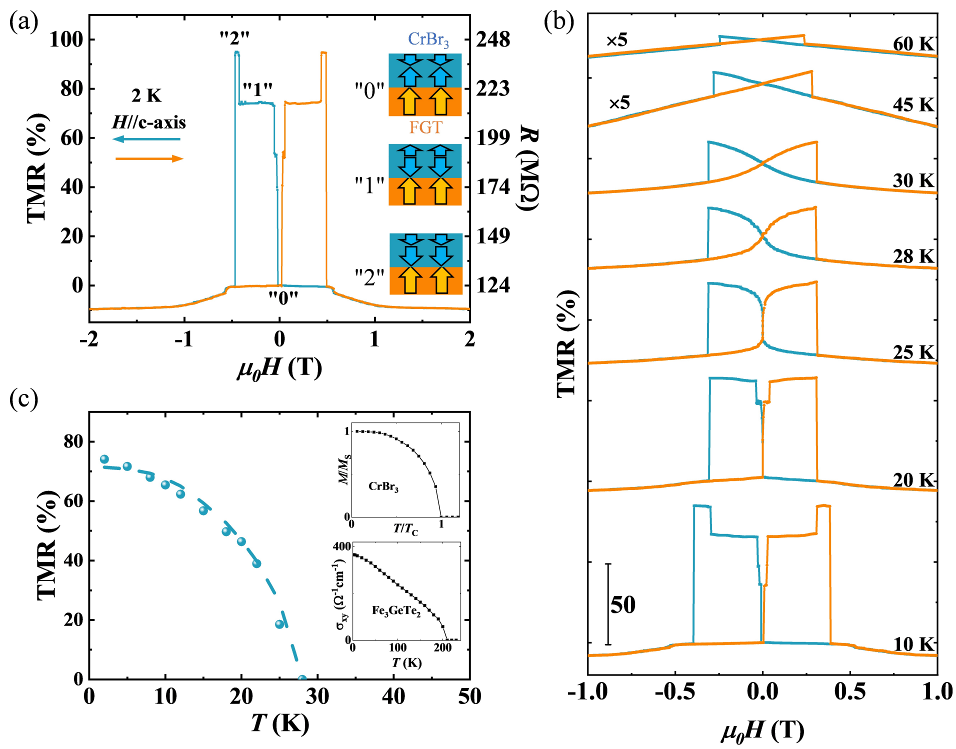

FIG. 2. **Large TMR in hybrid spin filter. (a)** Magnetic field dependence of tunneling resistance measured at 2 K with bias of -0.66 V, the magnetic field is applied along the c-axis of FGT and $CrBr_3$. The insets show the magnetic states of FGT and $CrBr_3$ that are corresponding to different resistance states. **(b)** TMR at different temperatures. For clarity, the data are vertically shift, TMR of 45 K and 60 K are amplified by 5 times. **(c)** Temperature dependence of TMR between resistance states "0" and "1", the dots are experimental data and the dashed line is the fitting data. The insets show the calculated spontaneous magnetization of $CrBr_3$ and measured temperature dependence of anomalous Hall conductivity in FGT.

value of our device reaches as high as 100% with the definition of TMR $= R_H/R_{0\text{T}} - 1$. A symmetric behavior is observed when the magnetic field is swept from negative to positive values, with the junction reaching a high resistance state at around 0.02 T and dropping to a low resistance state at around 0.5 T. It should be noticed that previous studies have demonstrated that the coercivity field of a few-layer $CrBr_3$ is tens of mT and the coercivity field of thin FGT is hundreds of mT, closely matching two featured magnetic field values (0.02 T and 0.5 T) in our measurements. This spin-valve-like TMR behavior in our device thus perfectly matches the theoretical proposal shown in Fig. 1(a), that is, a low resistance for parallel configuration and a high resistance for antiparallel configuration.

There is an additional feature in the high-resistance state. The tunneling resistance jumps from 223 MΩ to an even higher resistance (248 MΩ) at -0.43 T when the magnetic field sweeps from positive to negative value (at +0.43 T in the reverse sweep). For a clear description of the resistance states, we define the resistance state at zero field as "0", the relatively high resistance state as "1", and the highest resistance state as "2". The occurrence of the resistance state "2" is not expected if $CrBr_3$ is purely ferromagnetic. However, it can be understood if there is an interlayer antiferromagnetic coupling between two parts of $CrBr_3$, as scheduled in the inset of Fig. 2(a). The tunneling resistance changes from state "1" to "2" when the interlayer coupling changes from antiferromagnetic to ferromagnetic. Previous studies have pointed out that the interlayer magnetic coupling of Chromium trihalides depends on the interlayer stacking. The value of 0.43 T matches the spin-flip field observed in $CrBr_3$ with S-type stacking [38], thus strongly supporting the conclusion that our $CrBr_3$ is composed of antiferromagnetic parts. As discussed in the Supplementary Material [40], even with interlayer antiferromagnetic coupling between specific layers, the whole $CrBr_3$ still has a spin filtering effect similar to that of ferromagnets.

We further measured the TMR at different temperatures. The critical fields when the low- and high- resistance states switch (± 0.02 T, ± 0.5 T) shift to a lower magnetic field with increasing temperature, the same trend as the expected temperature dependence of coercivity field of ferromagnets (FGT and $CrBr_3$). The switch field between resistance states "1" and "2" (± 0.43 T at 2 K) also moves to a lower field at higher temperature and finally disappears above 28 K, same as $CrBr_3$ with S-type stacking[38]. The sharp transition from the resistance state "0" to "1" only persists below 28 K, consis-

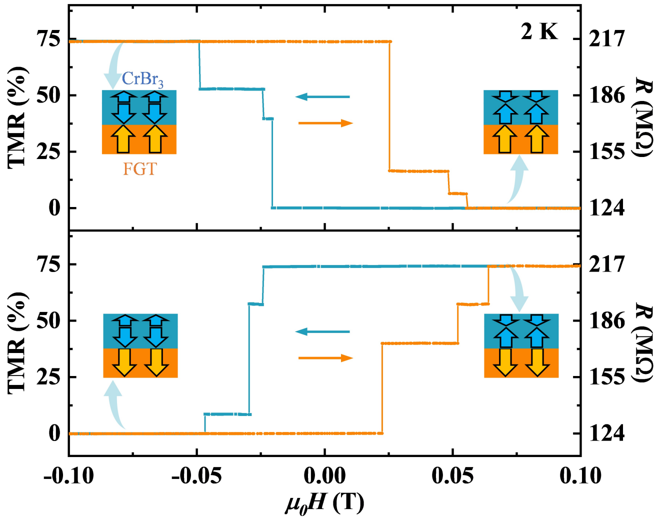

FIG. 3. **Non-volatile behavior of hybrid spin filter.** The upper (lower) part shows the magnetic field dependence of tunneling resistance when the magnetization of FGT is initialed into the up (down) status, small magnetic field (± 0.1 T) is used to control the magnetization of $CrBr_3$.

tent with the critical temperature of the thin $CrBr_3$ flake obtained from the RT curve in Fig. 1(c). This $CrBr_3$ flake becomes a paramagnet above 28 K, but its electronic band is still spin-split when an external magnetic field is applied, and the splitting energy is proportional to the magnetization induced by the magnetic field [36]. At the same time, the FGT flake is still a hard ferromagnet below 220 K. This results in a noticeable TMR even above 28 K as shown in Fig. 2(b), with sharp resistance changes at the coercivity field of FGT and smooth resistance changes between them. The temperature dependence of TMR between two well-defined resistance states "0" and "1" is summarized in Fig. 2(c), and it can be qualitatively fitted by the extended Jullière model as we will discuss later.

After demonstrating that large TMR is achieved, we show that our device is non-volatile. Fig. 3 summarizes the magnetoresistance data with a magnetic field swept in the small range that only changes the magnetization status of $CrBr_3$. The upper panel of Fig. 3 is the result when the magnetization of FGT was initiated into the up-state. When the positive (negative) magnetic field switches $CrBr_3$ magnetization into the up (down) status, the whole structure reaches the low (high) resistance state, and this low (high) resistance state persists after the magnetic field is removed, thus illustrating the non-volatility of our device. There are several resistance steps between 124 MΩ and 217 MΩ, this should be related to the lateral domains of $CrBr_3$ which have slightly different coercivity field [41]. The overall TMR behavior of our device is similar to that of the conventional magnetic tunnel junction, with FGT serving as the fixed layer and $CrBr_3$ working as the free layer that can be easily controlled with an external field.

The high quality of 2D hybrid spin filters allows for the tunability of TMR through bias voltage, as shown in Fig. 4(a). We observe that bias voltage not only tunes the amplitude of the TMR, but also reverses its sign. In addition to the TMR measured at separated bias voltage points, we also measured IV curves at different states, which are shown in the inset of Fig. 4(b). TMR calculated from IV curves are shown as solid lines in Fig. 4(b), which match well with the measurements with separated bias voltage shown as dots. We notice that there is finite TMR background in the parallel configuration above 0.5 T, and its sign does not change when the signs of TMR for state "1" and "2" are changed by the bias voltage. This TMR background is associated with the intrinsic TMR of $CrBr_3$ barrier and is discussed in detail in Supplementary Material[40].

We interpret the temperature and bias voltage dependence of TMR within the scenario of hybrid spin filter, whose TMR can be described by the extended Jullière model [42] with TMR $= 2P_1P_2/(1 - P_1P_2)$ (see Supplemental Material[40]). Here P_1 is the spin polarization of the ferromagnetic metal FGT, and P_2 is the spin polarization of the ferromagnetic semiconductor $CrBr_3$ due to the spin filtering effect, defined as $P_2 = (I_{\rm up} - I_{\rm down})/(I_{\rm up} + I_{\rm down})$. P_1 shows the same temperature dependence as anomalous Hall conductivity, which is proportional to the magnetization of FGT [27]. So $P_1(T) = \alpha \cdot M(T)_{\rm FGT}$, where α is a temperature independent constant determined by the intrinsic property of FGT. The measured temperature dependence of the anomalous Hall conductivity of FGT flake with similar thickness is shown in the inset of Fig. 2(c). We find that P_2 of an atomically thin ferromagnetic semiconductor is also proportional to its magnetization when the spin-split energy is small. $P_2(T) = \beta \cdot M(T)_{\rm CrBr_3}$, where β is a constant determined by the material and applied voltage, we detail this relationship in the Supplementary Material[40]. When the semiconductor is composed of two antiferromagnetically coupled ferromagnets (such as $CrBr_3$ in the resistance states "0" and "1"), its spin polarization has the same relation as that of a ferromagnetic semiconductor but with effective magnetization smaller than the sublattice. $P_2(T) = \beta{\cdot}\delta M(T)_{\rm CrBr_3}$, where δ is a constant smaller than 1 and is determined by the relative thickness of two antiferromagnetic coupled parts (see Supplementary Material[40]). Precise measurement of the thin $CrBr_3$ flake magnetization is technically not easy, and it was realized with graphene Hall bar micromagnetometry[32]. That result is well reproduced by the temperature dependence calculation in a mean-field treatment of the XXZ model [32]. The calculation of spontaneous magnetization is shown in the bottom inset of Fig. 2(c), we approximate $M(T)_{\rm CrBr_3}$ with this calculated value as the experimental magnetic field at state “1” is very small. So the temperature dependence of TMR in our hybrid spin filter is TMR$(T) = \frac{2\alpha M(T)_{\rm FGT}\cdot\beta\delta M(T)_{\rm CrBr_3}}{1-\alpha M(T)_{\rm FGT}\cdot\beta\delta M(T)_{\rm CrBr_3}} = \frac{2\gamma M(T)_{\rm FGT} M(T)_{\rm CrBr_3}}{1-\gamma M(T)_{\rm FGT} M(T)_{\rm CrBr_3}}$, where $\gamma = \alpha \cdot \beta\delta$ is the only fitting parameter for measured

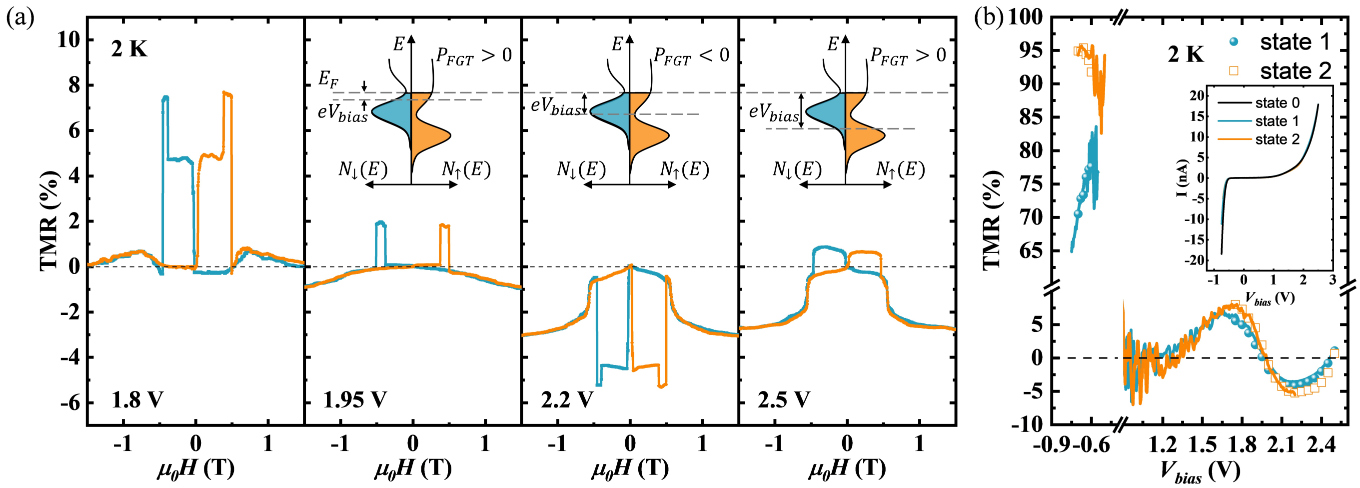

FIG. 4. **Bias-driven TMR polarity reversals in hybrid spin filter. (a)** Magnetic field dependence of tunneling resistance measured with different bias voltages at 2 K. The insets show more electronic states involve tunneling process with higher bias voltage, resulting in changes of sign of spin polarization. **(b)** Bias voltage dependence of TMR. The dots are TMR measured with separated voltages and the solid line is the TMR calculated from IV curves. The inset shows the IV curves measured at different states.

temperature dependence of TMR in our device. We can see that this model can fit the experimental data very well, indicated as the dashed line in Fig. 2(c).

The TMR polarity reversals with voltage bias can also be qualitatively interpreted with the extended Jullière model. FGT's electronic states at high energy levels will involve the tunneling process when a large bias voltage is applied, and the spin polarization of FGT will change between a positive value (majority-spin electrons dominate) and a negative value (minority-spin electrons dominate), as illustrated by insets of Fig. 4(a). This will result in TMR polarity reversals in our device, as the spin polarization of $CrBr_3$ is always positive. We calculate the spin polarization of FGT through its band structure and indeed find sign changes (see Supplementary Material[40]). However, the exact value of the bias voltage when TMR polarity switches does not match our experimental data well. We notice that TMR polarity reversals have also recently been observed in magnetic tunnel junctions with Fe_3GeTe_2 [29, 30] and Fe_3GaTe_2 [43]. In those systems, quantitative interpretation of the precise voltage of TMR sign changes is still challenging, which means a more dedicated model should be introduced. The TMR polarity switching from positive to negative and then back to positive appears to be easily obtained in vdW heterostructures, actually it is rarely reported in spintronic devices with conventional thin films. This may be because the spin-flip scattering process at the atomically sharp vdW interfaces can be minimized [29], highlighting the great potential of vdW 2D materials in controlling spin injection through the electric field.

In summary, we have fabricated high-quality hybrid spin filters with 2D magnetic metal FGT and semiconductor $CrBr_3$, whose tunneling resistance depends on the alignment of magnetizations of two magnets. TMR as large as 100% is obtained at low temperature and its temperature dependence can be interpreted with the extended Jullière model. The high-quality device enables the control of spin polarization through an electric field, which can expand the functionalities of this spintronic device. Unlike existing spin filters of 2D antiferromagnets, such as CrI_3 and CrSBr, our hybrid spin filters are nonvolatile, and thus they have great potential applications in future information technology, such as in-memory calculations. To achieve such applications, the operation temperature of the hybrid spin filter must be increased by using 2D ferromagnetic semiconductors and metals with high Curie temperatures [44, 45]. Additionally, exploring the electric method of switching magnetization is also essential, especially the spin-orbit torque with quantum materials [46–48]. Since the free layer of hybrid spin filter is a 2D magnetic semiconductor and all the switching current passes through the spin-orbit torque materials, the magnetization control could be more efficient compared to metal based devices [49, 50], thus making this type of device more compelling in future low energy consumption electronics.

ACKNOWLEDGEMENT

This work is financially supported by National Natural Science Foundation of China (Grants no. 12374121, 12304232, 12274090, 62274087 and 92265103), Shaanxi Fundamental Science Research Project for Mathematics and Physics (22JSY026,23JSQ011), the Fundamental Research Funds for the Central Universities, Anhui Provincial Major S&T Project (Contract No. s202305a12020005) and the Natural Science Foundation of Shanghai (Grant No.22ZR1406300). K.W. and T.T. acknowledge the support from the JSPS KAK-

ENHI (Grants no. 21H05233 and 23H02052) and World Premier International Research Center Initiative (WPI), MEXT, Japan. We thank Pei Zhou at Instrument Analysis Center, Liangliang Zhang and Manman Zhang at State Key Laboratory for Manufacturing Systems Engineering of Xi'an Jiaotong University for the technical support.

REFERENCES

[1] Žutić, I., Fabian, J. & Das Sarma, S. Spintronics: Fundamentals and applications. *Rev. Mod. Phys.* **76,** 323–410 (2004).

[2] Avsar, A. *et al.* Colloquium: Spintronics in graphene and other two-dimensional materials. *Rev. Mod. Phys.* **92,** 021003 (2020).

[3] Hirohata, A. *et al.* Review on spintronics: Principles and device applications. *J. Magn. Magn. Mater.* **509,** 166711 (2020).

[4] Tsymbal, E. Y., Mryasov, O. N. & LeClair, P. R. Spin-dependent tunnelling in magnetic tunnel junctions. *J. Condens. Matter Phys.* **15,** R109 (2003).

[5] Moodera, J. S., Santos, T. S. & Nagahama, T. The phenomena of spin-filter tunnelling. *J. Condens. Matter Phys.* **19,** 165202 (2007).

[6] Miao, G.-X., Müller, M. & Moodera, J. S. Magnetoresistance in double spin filter tunnel junctions with nonmagnetic electrodes and its unconventional bias dependence. *Phys. Rev. Lett.* **102,** 076601 (2009).

[7] LeClair, P. *et al.* Large magnetoresistance using hybrid spin filter devices. *Appl. Phys. Lett.* **80,** 625–627 (2002).

[8] Gajek, M. *et al.* Spin filtering through ferromagnetic $BiMnO_3$ tunnel barriers. *Phys. Rev. B* **72,** 020406(R) (2005).

[9] Gajek, M. *et al.* Tunnel junctions with multiferroic barriers. *Nat. Mater.* **6,** 296–302 (2007).

[10] Harada, T. *et al.* Spin-filter tunnel junction with matched fermi surfaces. *Phys. Rev. Lett.* **109,** 076602 (2012).

[11] Lüders, U. *et al.* $NiFe_2O_4$: a versatile spinel material brings new opportunities for spintronics. *Adv. Mater.* **18,** 1733–1736 (2006).

[12] Lüders, U. *et al.* Bias dependence of tunnel magnetoresistance in spin filtering tunnel junctions: Experiment and theory. *Phys. Rev. B* **76,** 134412 (2007).

[13] Ramos, A. V. *et al.* Room temperature spin filtering in epitaxial cobalt-ferrite tunnel barriers. *Appl. Phys. Lett.* **91,** 122107 (2007).

[14] Huang, B. *et al.* Layer-dependent ferromagnetism in a van der waals crystal down to the monolayer limit. *Nature* **546,** 270–273 (2017).

[15] Gong, C. *et al.* Discovery of intrinsic ferromagnetism in two-dimensional van der waals crystals. *Nature* **546,** 265–269 (2017).

[16] Song, T. *et al.* Giant tunneling magnetoresistance in spin-filter van der waals heterostructures. *Science* **360,** 1214–1218 (2018).

[17] Klein, D. R. *et al.* Probing magnetism in 2D van der waals crystalline insulators via electron tunneling. *Science* **360,** 1218–1222 (2018).

[18] Wang, Z. *et al.* Very large tunneling magnetoresistance in layered magnetic semiconductor CrI_3. *Nat. Commun.* **9,** 2516 (2018).

[19] Kim, H. H. *et al.* One million percent tunnel magnetoresistance in a magnetic van der waals heterostructure. *Nano Lett.* **18,** 4885–4890 (2018).

[20] Wang, Z. *et al.* Determining the phase diagram of atomically thin layered antiferromagnet $CrCl_3$. *Nat. Nanotechnol.* **14,** 1116–1122 (2019).

[21] Cai, X. *et al.* Atomically thin $CrCl_3$: an in-plane layered antiferromagnetic insulator. *Nano Lett.* **19,** 3993–3998 (2019).

[22] Klein, D. R. *et al.* Enhancement of interlayer exchange in an ultrathin two-dimensional magnet. *Nat. Phys.* **15,** 1255–1260 (2019).

[23] Huang, M. *et al.* Layer-dependent magnetism and spin fluctuations in atomically thin van der waals magnet $CrPS_4$. *Nano Lett.* **23,** 8099–8105 (2023).

[24] Lan, G. *et al.* Giant tunneling magnetoresistance in spin-filter magnetic tunnel junctions based on van der waals a-type antiferromagnet CrSBr. *Chin. Phys. Lett.* **40,** 058501 (2023).

[25] Deng, Y. *et al.* Gate-tunable room-temperature ferromagnetism in two-dimensional Fe_3GeTe_2. *Nature* **563,** 94–99 (2018).

[26] Fei, Z. *et al.* Two-dimensional itinerant ferromagnetism in atomically thin Fe_3GeTe_2. *Nat. Mater.* **17,** 778–782 (2018).

[27] Wang, Z. *et al.* Tunneling spin valves based on Fe_3GeTe_2/hBN/Fe_3GeTe_2 van der waals heterostructures. *Nano Lett.* **18,** 4303–4308 (2018).

[28] Zhu, W. *et al.* Large tunneling magnetoresistance in van der waals ferromagnet/semiconductor heterojunctions. *Adv. Mater.* **33,** 2104658 (2021).

[29] Min, K.-H. *et al.* Tunable spin injection and detection across a van der waals interface. *Nat. Mater.* **21,** 1144–1149 (2022).

[30] Zhu, W. *et al.* Large and tunable magnetoresistance in van der waals ferromagnet/semiconductor junctions. *Nat. Commun.* **14,** 5371 (2023).

[31] Ghazaryan, D. *et al.* Magnon-assisted tunnelling in van der waals heterostructures based on $CrBr_3$. *Nat. Electron.* **1,** 344–349 (2018).

[32] Kim, M. *et al.* Micromagnetometry of two-dimensional ferromagnets. *Nat. Electron.* **2,** 457–463 (2019).

[33] Kim, H. H. *et al.* Evolution of interlayer and intralayer magnetism in three atomically thin chromium trihalides. *Proc. Natl. Acad. Sci. U. S. A* **116,** 11131–11136 (2019).

[34] Wang, H., Eyert, V. & Schwingenschlögl, U. Electronic structure and magnetic ordering of the semiconducting chromium trihalides $CrCl_3$, $CrBr_3$ and CrI_3. *J. Condens. Matter Phys.* **23,** 116003 (2011).

[35] Soriano, D., Katsnelson, M. I. & Fernández-Rossier, J. Magnetic two-dimensional chromium trihalides: A theoretical perspective. *Nano Lett.* **20,** 6225–6234 (2020).

[36] Wang, Z. *et al.* Magnetization dependent tunneling conductance of ferromagnetic barriers. *Nat. Commun.* **12,** 6659 (2021).

[37] Chen, W. *et al.* Direct observation of van der waals stacking–dependent interlayer magnetism. *Science* **366,** 983–987 (2019).

[38] Yao, F. *et al.* Multiple antiferromagnetic phases and magnetic anisotropy in exfoliated $CrBr_3$ multilayers. *Nat. Commun.* **14,** 4969 (2023).

[39] Yang, S. *et al.* Controlling the 2D magnetism of $CrBr_3$ by van der waals stacking engineering. *J. Am. Chem. Soc.* **145,** 28184–28190 (2023).

[40] See the Supplemental Material [url] for additional experimental details, magnetoresistance (MR) data of another device, and the theoretical derivations of the extended Jullière model and spin polarizations for $CrBr_3$ and FGT, which include Refs [51–54].

[41] Sun, Q.-C. *et al.* Magnetic domains and domain wall pinning in atomically thin $CrBr_3$ revealed by nanoscale imaging. *Nat. Commun.* **12,** 1989 (2021).

[42] Julliere, M. Tunneling between ferromagnetic films. *Phys. Lett. A* **54,** 225–226 (1975).

[43] Jin, W. *et al.* Room-temperature and tunable tunneling magnetoresistance in Fe_3GaTe_2-based 2D van der waals heterojunctions. *ACS Appl. Mater. Interfaces* **15,** 36519–36526 (2023).

[44] Bonilla, M. *et al.* Strong room-temperature ferromagnetism in VSe_2 monolayers on van der waals substrates. *Nat. Nanotech.* **13,** 289–293 (2018).

[45] Zhang, G. *et al.* Above-room-temperature strong intrinsic ferromagnetism in 2D van der waals Fe_3GaTe_2 with large perpendicular magnetic anisotropy. *Nat. Commun.* **13,** 5067 (2022).

[46] Mak, K. F., Shan, J. & Ralph, D. C. Probing and controlling magnetic states in 2D layered magnetic materials. *Nat. Rev. Phys.* **1,** 646–661 (2019).

[47] Wu, H. *et al.* Magnetic memory driven by topological insulators. *Nat. Commun.* **12,** 6251 (2021).

[48] Tiwari, S., Van de Put, M. L., Temst, K., Vandenberghe, W. G. & Sorée, B. Atomistic modeling of spin and electron dynamics in two-dimensional magnets switched by two-dimensional topological insulators. *Phys. Rev. Appl.* **19,** 014040 (2023).

[49] Gupta, V. *et al.* Manipulation of the van der waals magnet $Cr_2Ge_2Te_6$ by spin–orbit torques. *Nano Lett.* **20,** 7482–7488 (2020).

[50] Ostwal, V., Shen, T. & Appenzeller, J. Efficient spin-orbit torque switching of the semiconducting van der waals ferromagnet $Cr_2Ge_2Te_6$. *Adv. Mater.* **32,** 1906021 (2020).

[51] Wang, Y. *et al.* Anisotropic anomalous hall effect in triangular itinerant ferromagnet Fe_3GeTe_2. *Phys. Rev. B* **96,** 134428 (2017).

[52] Dumcenco, D. & Giannini, E. Growth of van der waals magnetic semiconductor materials. *J. Cryst. Growth* **548,** 125799 (2020).

[53] Wang, L. *et al.* One-dimensional electrical contact to a two-dimensional material. *Science* **342,** 614–617 (2013).

[54] Santos, T. S. *et al.* Determining exchange splitting in a magnetic semiconductor by spin-filter tunneling. *Phys. Rev. Lett.* **101,** 147201 (2008).